JOURNAL OF SOLID STATE CHEMISTRY 48, 21–32 (1983)

Structure of γ-Fe_2O_3 Microcrystals: Vacancy Distribution and Superstructure

M. BOUDEULLE,* H. BATIS-LANDOULSI,† CH. LECLERCQ,‡ AND P. VERGNON

Laboratoire de Catalyse Appliquée et Cinétique Hétérogène de l'Université Claude Bernard (Lyon I) associé au CNRS (L.A. N° 231), 43 boulevard du 11 novembre 1918, 69622 Villeurbanne Cedex, France

Received September 27, 1982; in revised form December 9, 1982

Well-crystallized particles of γ-ferric oxide, prepared by a vapor phase reaction, have been studied by means of X rays and electron diffraction. A statistical distribution of iron vacancies inside the cubic spinel structure is dismissed. The vacancy ordering leads to a cubic superstructure with a threefold unit cell. However, different degrees of vacancy ordering can be observed. Moreover, the occurrence of plateletlike crystals has allowed us to recognize intermediate states between the γ- and α—Fe_2O_3 structures. The importance of preparative conditions is clearly established.

Introduction

Like Al_2O_3 or Mn_2O_3, ferric oxide may crystallize with two structures; the γ cubic form transforms, in a monotropic way, into the more stable α form, which has a rhombohedral lattice.

The ferrimagnetic γ form is generally prepared by dehydration of the corresponding oxyhydroxide γ-FeOOH (lepidocrocite) or by oxidation at low temperature of magnetite, Fe_3O_4. Hägg (*1*) and Verwey (*2*) have studied its structure independently using X-ray diffraction powder data; they proposed that γ-Fe_2O_3 has the same inverse spinel structure as magnetite, but with cation vacancies since $21\frac{1}{3}$ iron atoms instead of 24 would be located in 8 tetrahedral and 16 octahedral holes of the oxygen close-packed lattice. The vacancies ($2\frac{2}{3}$) were assumed to be randomly distributed in the octahedral sites occupied by iron in magnetite. The resulting space group remains $Fd3m$, as for the ideal spinel structure.

Néel (*3*), from the calculation of the saturation magnetization, concluded that the vacancies were located in the octahedral cation sites of the spinel structure ($16d$). Braun (*4*) proposed that the same symmetry ($P4_332$ or $P4_132$) appears in γ-Fe_2O_3 as in $LiFe_5O_8$, hydrogen ions being trapped in the cation vacancies. This conclusion is supported by (i) the existence of a number of extra reflections (forbidden by the spinel

* Laboratoire de Cristallographie et Chimie des Matériaux associé au CNRS (E.R.A. N° 600), 43 boulevard du 11 novembre 1918, 69622 Villeurbanne Cedex, France.

† Present address: Département de Chimie, Faculté des Sciences, Université de Tunis, Tunisie.

‡ Institut de Recherches sur la Catalyse, CNRS, 2, avenue Albert Einstein, 69626 Villeurbanne Cedex, France.

0022-4596/83 $3.00

space group) in the X-ray powder pattern (*4, 5*), which also occur in the diagram of the ordered lithium ferrite $Fe_8[Li_4Fe_{12}]O_{32}$ (the square brackets denote the cations in octahedral sites), and (ii) the fact that the stability of γ-Fe_2O_3 seems to be connected with the presence of water (*2, 6*).

Later, Van Ossterhoot and Rooijmans (*7*) observed that the repartition of $Fe_8[Fe_{4/3}\square_{8/3}Fe_{12}]O_{32}$ gives the same extra reflections. Moreover, all the reflections could be indexed using a tetragonal unit cell, having $c/a = 3$ and $a = 8.33$ Å. The absence of the reflections $00l$ with $l \neq 4n$ points to a fourfold screw axis with a translation $\vec{c}/4$.

Neutron diffraction data (*8*) support the preferential distribution of vacancies in the octahedral sites *only*. A large number of studies deal with the vacancy location and distribution. A general review is presented by Morrish (*9*). Some divergences exist in the literature concerning the extra lines in the X-ray patterns, suggesting that the cation distribution could differ according to the preparation mode. Unfortunately, the difficulty in growing well-defined and "homogeneous" crystals of γ-Fe_2O_3 has prevented workers from obtaining unambiguous data. That is the main reason for the lack of significant structural results in this area.

Submicronic crystals of γ-Fe_2O_3 with well-defined morphology can be prepared, under controlled conditions, by vapor phase reaction in a hydrogen–oxygen flame (*10*). It seemed of interest to study these oxide particles by means of the most appropriate techniques of investigation, electron microscopy (*11*) and diffraction, to gain more information about the γ-Fe_2O_3 structure.

Preparation and Characterization of γ-Fe_2O_3

The preparation of α- and γ-Fe_2O_3 from a flame supported reaction has been previously described (*10*). Nonporous oxide particles are obtained by hydrolysis and/or oxidation of corresponding chloride vapor in an oxygen–hydrogen flame. The changes of the thermodynamic and kinetic reaction parameters allow us to control the structural and morphological properties of the oxide particles. The γ-Fe_2O_3 studied in this work has been prepared in a flame at 3000 K. Solid particles result from the quenching of intermediate liquid droplets.

The mean size of particles calculated from the BET surface area (16.5 $m^2\ g^{-1}$), is 76 nm. Their morphological properties have been described in detail elsewhere (*11*). The γ-Fe_2O_3 particles are well-crystallized, single and twinned cubic crystals, as shown by electron microscopy, using lattice imaging coupled with selected area electron diffraction.

The {111}, {100}, and {110} faces are most common, generally in association, resulting in a rhombocuboctahedron. The (110) faces appear often stepped by (111) planes. A few of the crystals (about 1%) are thin triangular or hexagonal platelets.

The X-ray powder diagram is characteristic of γ-Fe_2O_3 (ASTM = 4-0755). No changes are observed in this diagram when the oxide is heated at 573 K for 15 hr. Under these conditions, IR spectroscopy shows that only traces of surface hydroxyl groups are present.

Thermal treatments for a period of 15 hr above 673 K cause the appearance of α-Fe_2O_3 lines in the X-ray diagram. At 723 K (15 hr), γ-Fe_2O_3 is completely transformed into α-Fe_2O_3. The differential thermal analysis plot reveals an exothermic phenomenon at 723 K: the measured heat of transformation is 13.8 kJ $mole^{-1}$, in good agreement with the value obtained by Ferrier (*12*) corresponding to the $\gamma \rightarrow \alpha$ topotactic transition (*13*).

A Mössbauer spectrum (Fig. 1) taken at room temperature (with a 100 mCi ^{57}Co/Pt

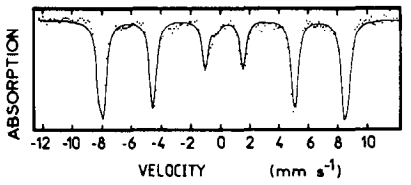

FIG. 1. Mössbauer spectrum of γ-Fe_2O_3 prepared in a flame.

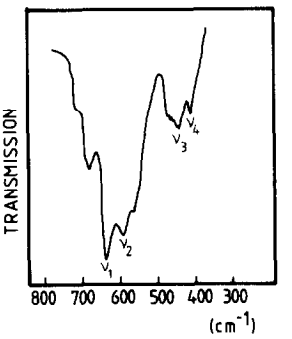

FIG. 2. Infrared spectrum of γ-Fe_2O_3 prepared in a flame.

source) shows the hyperfine split pattern characteristic of γ-Fe_2O_3 (*14*). The hyperfine fields at iron nuclei on tetrahedral and octahedral sites are almost equal and the Mössbauer patterns overlap. The fit of the spectrum allows calculation of a value of 502 kOe, in agreement with the values of fields obtained from several other experiments (*15–17*). The isomeric shift of 0.5 mm sec^{-1} (with respect to N.P.S.) characterizes the Fe^{3+} ions. The absence of quadrupolar interaction results from the cubic crystalline symmetry. The saturation mag-

TABLE I

CALCULATED STRUCTURE FACTORS FOR VARIOUS ARRANGEMENTS OF VACANCIES IN γ-Fe_2O_3

		F_{cal}				
		$Fd3m$ statistical distribution on the octahedral sites	$P\bar{4}3m \equiv P23$ statistical distribution		$P4_332 \equiv P2_13$ statistical distribution	
hkl	F_{obs}		on 4 sites[a]	on 12 sites[b]	on 4 sites[c]	on 12 sites[d]
110	21.8		22.56	8.05	22.98	8.10
111	36.2	42.02	16.81	17.86	17.13	17.98
210	39.0		0	0	31.11	10.97
211	37.5		21.29	7.59	21.69	7.65
220	127.8	129.14	124.14	132.43	126.48	133.30
300	19.8		28.88	10.29	0	0
221	19.8		28.88	10.29	0	0
310	33.3		20.14	7.18	20.52	7.23
311	176.1	207.36	183.35	195.78	187.03	197.08
222	0	86.99	63.29	67.39	64.48	67.84
400	211.5	242.74	194.24	207.09	197.89	208.46
331	0	30.43	13.58	14.43	13.84	14.53
422	94.1	94.77	101.64	108.43	103.35	109.15
511	149.2	153.31	151.44	161.49	154.29	162.57
333	149.2	153.31	151.44	161.49	154.29	162.57
521	45.9		15.88	5.66	16.18	5.70
440	311.6	532.72	335.04	357.32	341.35	359.69

[a] (c) for $P23$ and $P\bar{4}3m$ (International Tables for X-ray Crystallography).
[b] (j) for $P23$ and (i) for $P\bar{4}3m$.
[c] (a) for $P2_13$ and (b) for $P4_332$.
[d] (b) for $P2_13$ and (d) for $P4_332$.

netization at 77 K is 1.15 μ_B, less than the value predicted by the Néel model (1.25 μ_B) (*3*).

Structural Study

1. X-ray Diffraction

As with the X-ray powder pattern, which contains all the lines of magnetite, the IR spectrum (Fig. 2) exhibits the four fundamental modes of the spinel structure (*18–20*). However, in both spectra, a few extra lines, forbidden for the ideal spinel structure, are present; they lead us to propose some arrangement of cation vacancies generating a lower symmetry structure within the same unit cell, or a superstructure.

Statistical vacancy distributions, described by subgroups of the spinel $Fd3m$ space group, were tested, assuming the lattice mode became primitive, to explain the observed 110, 210, 211, . . . reflections (Table I). Only the $P\bar{4}3m$ (or $P23$) and $P4_432$ (or $P2.3$) groups are compatible with the atomic positions of the spinel structure. Major discrepancies between the observed and calculated structure factors (with oxygen atoms in ideal positions) occur, as shown in Table I. No statistical distribution of vacancies could be fitted within the single cell with cubic symmetry.

However, it should be pointed out that the observed structure factors are derived from X-ray powder diffraction data, which correspond to mean values. As noted previously, different sets of extra lines have been reported and different vacancy schemes are certainly possible. Under these conditions, X-ray diffraction cannot be used successfully; such a study should be performed using electron diffraction on single crystals.

2. Electron Diffraction

Electron diffraction patterns observed on microcrystals with well-defined shapes and perfect structural integrity, as shown by lattice plane imaging, have suggested two kinds of vacancy distribution.

Statistical distribution of vacancies. Some crystals exhibit only the reflections corresponding to the F cubic lattice of the spinel unit cell (a = 8.33 Å). Others show a P cubic lattice with the same dimensions. The crystals are thick (50 to 100 nm) and the images are generally limited to a few reflections. In these cases, it is not possible to derive reliable information about the vacancy distribution from the observed intensities, and no conclusions in addition to the X-ray data can be drawn. It was confirmed, however, that a statistical distribution of the cation vacancies could occur in two ways: (i) all the octahedral sites are involved and the F lattice of the spinel structure is preserved, and (ii) the lattice becomes primitive and, according to the above calculations (Table I), the cubic symmetry is reduced.

Ordered distribution of vacancies. For several polyhedral and plateletlike crystals from the same sample, extra reflections indicate a cubic superstructure, with $a = 3a$ (Fig. 3, (100)* plane). The large cell contains 72 vacant positions. A vacancy ordering, resulting in a long-range order, is so established.

No space group could be derived from the bidimensional patterns, nor any information about the lattice mode since different types of extinctions are observed, and especially on the platelet crystals giving (111)* photographs.

The most common patterns show the reflections allowed by the spinel structure, together with spots based on the superstructure cell, for example, $(8\ \bar{4}\ \bar{4})$ (the corresponding spacing is actually equivalent to d_{110} of the α form) (Fig. 4a).

Other extra reflections were also observed depending on the crystal. Complex photographs exhibited two kinds of reflections: those corresponding to the P mode of

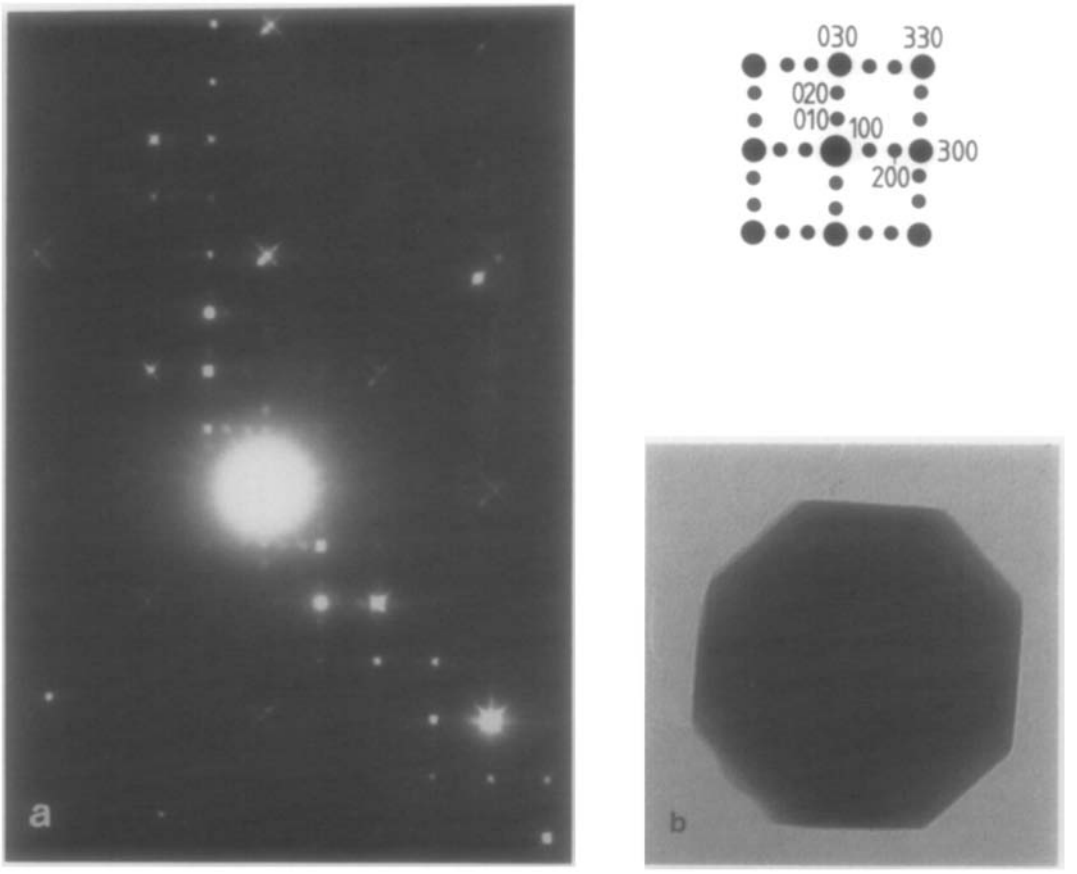

FIG. 3. (a) Electron diffraction pattern in [001] orientation from a polyhedral crystal of γ-Fe_2O_3 showing the superstructure (smaller spots, $a = 3a$). (b) Micrograph of the corresponding crystal.

the spinel structure, such as (1 $\bar{1}$ 0) or (2 $\bar{1}$ $\bar{1}$), noted (3 $\bar{3}$ 0) and (6 $\bar{3}$ $\bar{3}$) in the superstructure cell; and fractionary spots showing evidence of this superstructure (Figs. 4b,c).

In all cases, threefold symmetry is preserved and the resulting lattice mode is I since only reflections with $h + k + l = 2n$ are noticeable.

The plateletlike crystals are very important with respect to the development of the crystalline formation of ferric oxide. Unlike the polyhedral particles, these few crystals cannot result from an intermediate liquid state; they are developed directly from the vapor phase and their residence time in the hot zone of the flame varies, leading to different states of crystalline arrangement (some of them have the symmetry of α-Fe_2O_3) and, in particular, to different degrees of vacancy ordering. So, several stages have been observed, from the lowest to the highest degree of order, corresponding, respectively, to the maximum and the minimum (i.e., the α phase) of internal energy. Because of the correspondence between the lattices of the two polymorphs, especially in the direction normal to the ternary axis, it is difficult to differentiate between the α or γ form simply from geometrical considerations; the intensities of the reflections and their distribution should be taken into account.

The images identified as belonging to the

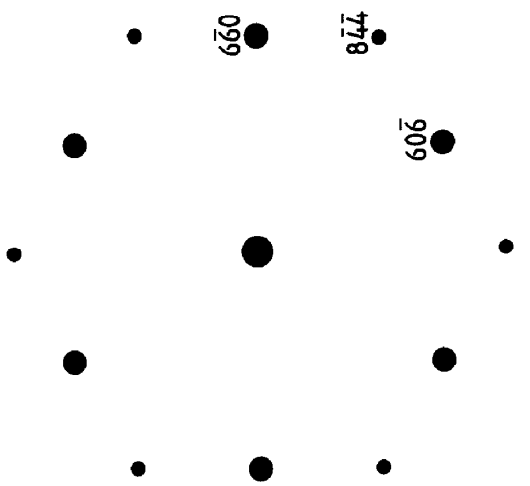
$0\bar{6}0$
$8\bar{4}\bar{4}$
$\bar{2}09$


a

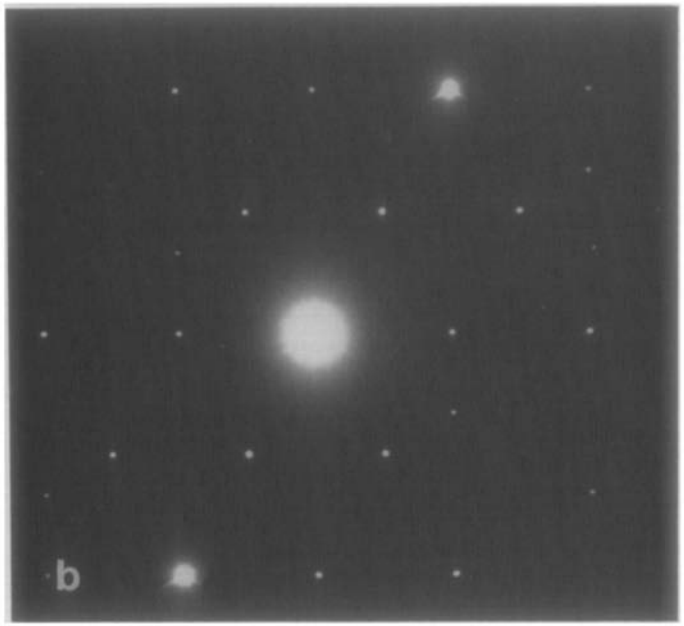

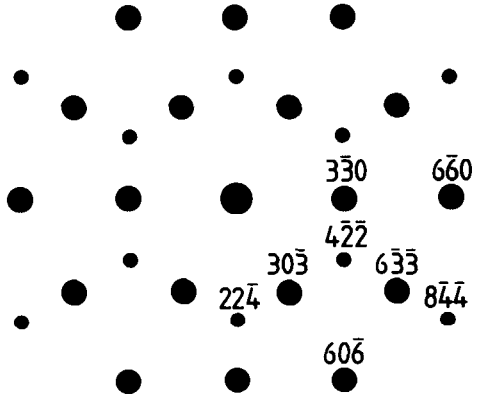

FIG. 4 (a–c). Electron diffraction patterns in [111] orientation (cubic notation) from platelets of γ-Fe_2O_3 due to different vacancy ordering. The smaller spots correspond to the superstructure.

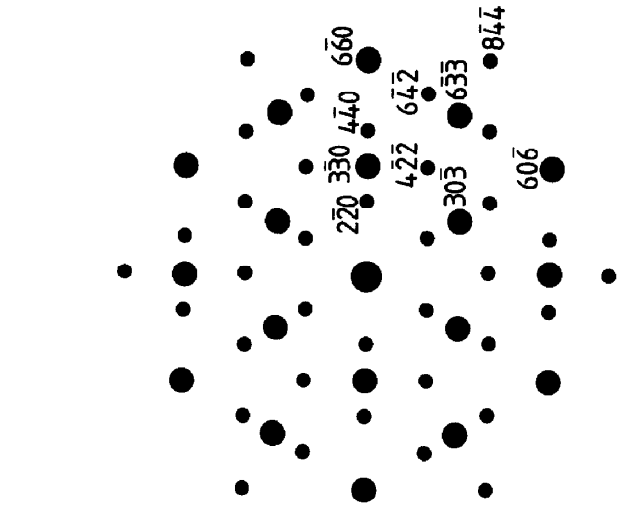

FIG. 4—*Continued.*

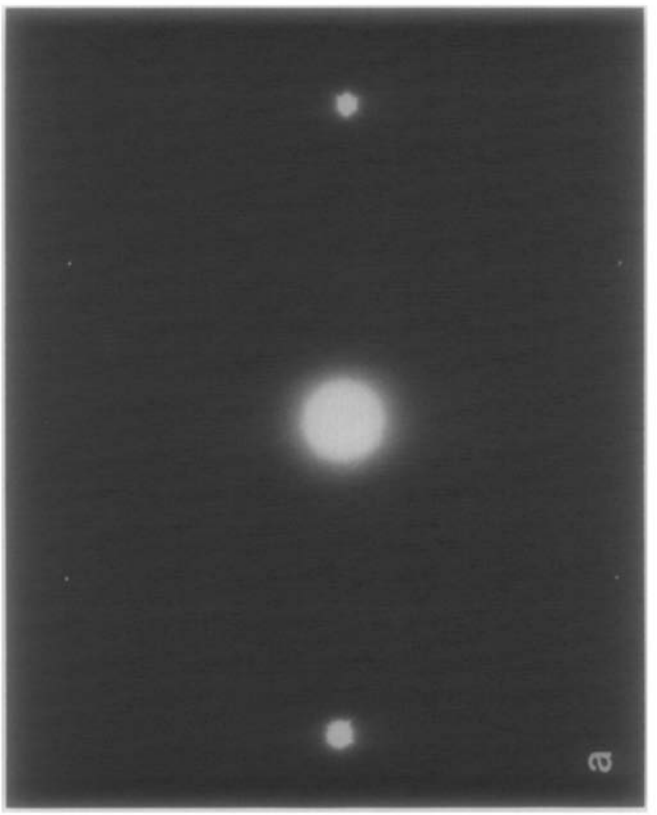

FIG. 5(a–c). Electron diffraction patterns from platelets of α-Fe_2O_3 (a) with rhombohedral structure ([00.1] orientation); (b,c) with two different cation distributions ([001] orientation, orthorhombic notation). The smaller spots correspond to the superstructure.

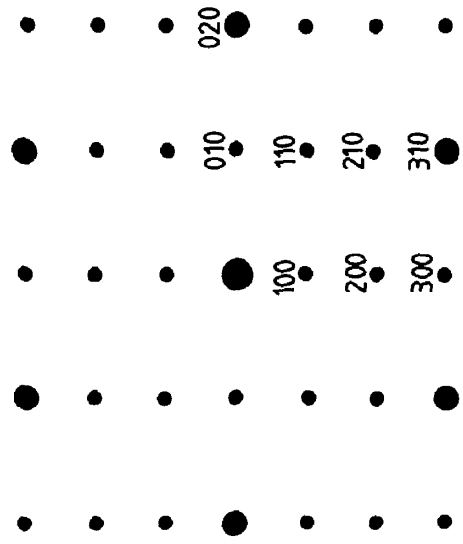

FIG. 5—*Continued.*

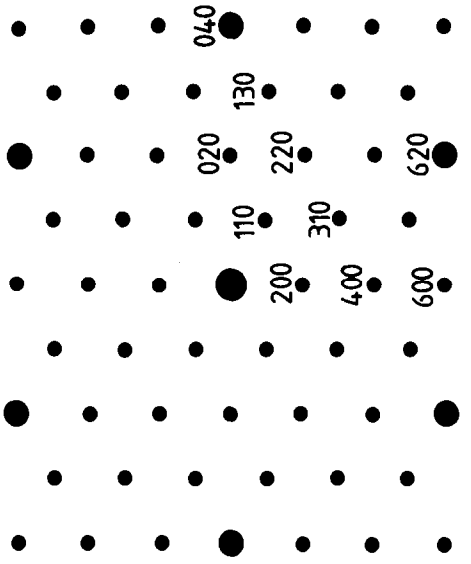

FIG. 5—*Continued.*

α form correspond to the orthohexagonal lattices derived from the (0 0 0 1)* direction of the α form (Fig. 5a) with (i) the disappearance of the reflection conditions ($-h + k + l = 3n$) which is characteristic of the rhombohedral lattice of the ideal hematite structure, and (ii) extra faint spots with the intensity distribution becoming twofold. In one case (Figs. 5b,c), the doubling of the period occurs parallel to the [100]* direction; the resulting unit cell is

$$a' = a_{(\alpha)}\sqrt{3} \qquad b' = a_{(\alpha)}.$$

The symmetry is $2mm$. In the other case (Fig. 7c), the doubling occurs in the two directions

$$a' = 2a_{(\alpha)}\sqrt{3} \qquad b' = 2a_{(\alpha)}$$

and the symmetry becomes $C2mm$.

Concluding Remarks

No evidence exists in the literature for the growth of large single crystals of γ-Fe_2O_3 suitable for a single-crystal X-ray structure determination. The preparation of this oxide by vapor phase reaction yielded microcrystals for which the electron diffraction was used for structural investigation.

Extra lines in the X-ray and IR spectra indicate that the hypothesis of a statistical distribution of the iron vacancies in the octahedral sites of a spinel structure fails. In fact, the vacancy distribution is either "statistical," with noncubic symmetry, or ordered, leading to a cubic superstructure with a threefold unit cell, for which a particular ordering cannot be proposed, due to the lack of bulk structural data.

From the examination of plateletlike particles, the morphology of which is compatible with both the α and γ forms, it has been possible to observe different stages of the cation vacancy ordering within the γ-Fe_2O_3 superstructure and/or to indicate intermediate states between γ- and α-Fe_2O_3.

In conclusion, evidence is given that the vacancy ordering depends on the preparative conditions in crystal growth and this observation explains the discrepancies of literature data concerning the extra lines observed on X-ray diagrams.

References

1. G. Hägg, *Z. Phys. Chem.* **29,** 88 (1935).
2. E. J. W. Verwey, *Z. Kristallogr.* **91,** 65 (1935).
3. L. Néel, *Ann. Phys.* **3,** 137 (1948).
4. P. B. Braun, *Nature (London)* **170,** 1123 (1952).
5. R. Haul and T. Schoon, *Z. Phys. Chem.* **44,** 216 (1939).
6. E. Kordes, *Z. Kristallogr.* **91,** 193 (1935).
7. G. W. Oosterhout and C. J. M. Rooijmans, *Nature (London)* **181,** 44 (1958).
8. G. A. Ferguson and M. Hass, *Phys. Rev.* **112,** 1130 (1958).
9. A. H. Morrish, "Crystals 2," p. 173, Springer-Verlag, Berlin (1980).
10. P. Vergnon and H. Batis-Landoulsi, *I & EC. Prod. Res. Dev.* **19,** 147 (1980).
11. H. Batis-Landoulsi, Ch. Leclercq, and P. Vergnon, *J. Electron Spectrosc. Microsc.* **7,** 149 (1982).
12. M. A. Ferrier, *C.R. Acad. Sci. Paris Ser. C* **264,** 819 (1967).
13. J. D. Bernal and A. L. Mackay, *Tschermaks Mineral Petrogr. Mitt.* **10,** 331 (1965).
14. H. Topsøe, J. A. Dumestic, and M. Boudart, *J. Phys. C-6* **35,** 411 (1974).
15. R. Bauminger, S. G. Cohen, A. Marinov, S. Ofer, and E. Segal, *Phys. Rev.* **122,** 1447 (1961).
16. W. H. Kelly, V. J. Folen, M. Haas, W. N. Slhreiner, and G. B. Beard, *Phys. Rev.* **124,** 80 (1961).
17. Y. Imaoka, Y. Hoshino, and M. Satoh, "Proc. Inst. Conf. on Ferrites Tokyo," p. 467, Univ. Tokyo Press, Tokyo (1971).
18. S. T. Hafner, *Z. Kristallogr.* **115,** 331 (1961).
19. W. B. White and B. A. de Angelis, *Spectrochim. Acta Part A* **23,** 985 (1971).
20. J. Preudhomme and P. Tarte, *Spectrochim. Acta Part A* **27,** 1817 (1971).